On the potential of ultrasound elastography for pressure ulcer early detection

Jean-François Deprez[a)] and Elisabeth Brusseau
CREATIS Laboratory, Université de Lyon, Insa de Lyon, Université Lyon 1, CNRS UMR5220,
Inserm U1044, Villeurbanne 69621, France

Jérémie Fromageau and Guy Cloutier
Laboratory of Biorheology and Medical Ultrasonics, University of Montreal Hospital Research Center
(CRCHUM), Montreal, Québec H2L 2W5, Canada

Olivier Basset
CREATIS Laboratory, Université de Lyon, Insa de Lyon, Université Lyon 1, CNRS UMR5220,
Inserm U1044, Villeurbanne 69621, France

Purpose: Pressure ulcers are areas of soft tissue breakdown induced by a sustained mechanical stress that damages the skin and underlying tissues. They represent a considerable burden to the society in terms of health care and cost. Yet, techniques for prevention and detection of pressure ulcers still remain very limited. In this article, the authors investigated the potential of ultrasound elastography for pressure ulcer early detection. Elastography is an imaging technique providing local information on biological tissue mechanical properties. It is relevant for pressure ulcer detection as this pathology is associated with a gradual stiffening of damaged tissues, beginning in the deeper tissues and progressing toward the skin surface.

Methods: A 2D ultrasound elastography method was proposed and its ability in terms of pressure ulcer detection was validated through numerical simulations and physical acquisitions on pressure ulcer mimicking phantoms. *In vivo* experiments on a rat model are also reported. A maintained pressure was applied on the animal thigh, with a view to generate a pressure ulcer, and ultrasound data were acquired and processed before and after application of this pressure.

Results: Numerical simulations demonstrated that a pressure ulcer can theoretically be detected at a very early stage with ultrasound elastography. Even when the ulcer region was characterized by a low stiffening (ratio of 1.8 relative to normal tissues), the corresponding elastogram clearly underlined the pathological area. This observation was confirmed by the results obtained on a physical phantom mimicking a pressure ulcer at an early stage. Computed elastograms showed strain differences between areas mimicking healthy and pathological tissues. Results corresponding to *in vivo* experiments revealed a difference in the way tissues behaved before and after the pressure was applied on the animal thigh, which strongly suggests the presence of a pathological area.

Conclusions: Experiments demonstrated that ultrasound elastography is a promising technique for pressure ulcer detection, especially at an early stage of the pathology, when the disease is still visually undetectable. In the absence of any gold standard method, this is also a first step toward the development of a quantitative technique. © *2011 American Association of Physicists in Medicine*.
[DOI: 10.1118/1.3560421]

Key words: pressure ulcer, ultrasound, elastography, medical imaging

I. INTRODUCTION

Pressure ulcers, or bedsores, are areas of soft tissue breakdown induced by a sustained mechanical stress that damages the skin and underlying tissues. They often appear after a prolonged period of immobility, during which biological tissues undergo a maintained pressure from a support (generally a bed or a wheelchair). Pressure ulcers mostly affect people with sensitivity loss or limited mobility, who are unable to feel and/or release the pressure. Elderly people, patients in hospital recovery and persons with spinal cord injury are especially at risk.

Few statistics are available to estimate the extent of this pathology. In 2001, wide variations were found for the prevalence of pressure ulcer in the United States:[1] 10%–18% in acute care, 2.3%–28% in long-term care, and 0%–29% in home care. In the United Kingdom, prevalence was estimated at 18% in 1993.[2] As life expectancy increases in western countries, this disease becomes a growing issue and represents a considerable burden to the society in terms of health care and associated cost.[3,4]

Despite these numbers, techniques for prevention and detection of pressure ulcer still remain very limited. For instance, risk scales do exist but they are mostly used for hospitalized patients, and their efficiency is largely questioned.[5]

Thus, detection and prevention are mainly based on the experience of the health-care personnel.

Different approaches were developed to study skin wounds. A good review of wound measurement techniques can be found in Ref. 6. These techniques can be divided into two categories: Visual assessment tools, based on color and digital image analysis, and physiological-based tools (i.e., blood flow, force, or pressure measurements). More recently, Weber *et al.*[7] developed a device to map the electrical impedance of a wound in order to determine the wound severity. Treuillet *et al.*[8] also presented an original approach to build 3D models of skin wounds from digital camera snapshots, allowing quantitative measurements of the wound, such as surface, depth, or volume.

Attempts to develop quantitative techniques for detection or prevention of pressure ulcers are far less numerous. In Ref. 9, 15 pressure ulcers were examined using four different noninvasive techniques: Skin temperature, redness index, skin retraction time, and ultrasound (US) scanning. Results showed that temperature and retraction time could not alone characterize the ulceration stage, while a redness index was useful in some cases. Ultrasound image processing could detect a subepidermal layer, which may be a good indicator that the skin is at risk. One can finally cite Ref. 10, where prevention of pressure ulcer was based on both movement measurement and autonomous nervous system analysis. Even though these studies were constructive, it is still relevant to develop new quantitative approaches.

This lack of quantitative assessment tools is likely the result of a limited understanding of the pathology itself. There is indeed very little literature on the process that triggers the formation of pressure ulcers.

To date, the most established theory is that tissue compression locally results in the occlusion of blood capillaries.[11–13] The mechanism leading to the formation of a pressure ulcer is linked with a shortage of blood supply, called ischemia, which prevents the natural exchanges of oxygen and nutrients. If the microcirculatory flow disturbance remains for too long, the ischemic condition leads to cell death and tissue damages.

It is also acknowledged that pressure ulcers are associated with a stiffening of damaged tissues, as shown in Refs. 14 and 15 on a rat model and on a realistic numerical model of human buttocks, respectively.

Finally, recent studies suggest that pressure ulcers can form either superficially or within deep tissues.[11,16,17] Superficial pressure ulcers arise in the skin. They are mainly caused by shear stresses and are easily detected by careful skin inspection. On the other hand, deep pressure ulcers (also called deep tissue injuries) develop in deep muscle layers covering bony prominences and are caused by sustained compression of the tissues. They follow a "deep-to-superficial" pattern and progress toward the skin surface. Therefore, severe necrosis of subcutaneous tissues may occur while the skin shows only minor signs of tissue breakdown. Consequently, deep ulcers are very difficult to identify. Since deep pressure ulcers are characterized by stiffening and a deep-to-superficial growing process, providing information on tissue local mechanical properties could be of major interest for physicians.

Accordingly, US elastography is proposed for pressure ulcer early detection. US elastography[18,19] is indeed providing to clinicians information on the local mechanical properties of soft biological tissues. This information, generally displayed as an image, enables the detection of unexpected stiff area within healthy tissues. Typical applications of US elastography are targeted to diseases such as breast and prostate cancer,[20,21] liver fibrosis,[22] and atherosclerosis.[23]

Potentially, pressure ulcer US elastography could be used for diagnosis and wound healing follow-up. US elastography also has the advantage of being noninvasive, low-cost, and portable.

In this paper, we investigated the potential of quasistatic US elastography for pressure ulcer early detection. The paper is organized as follows. Section II provides a description of the US elastography method, followed by its application to numerical data in Sec. III, and to a pressure ulcer mimicking phantom in Sec. IV. Section V is dedicated to the presentation of results obtained during an *in vivo* experiment. The final section provides a critical discussion and concluding remarks.

II. METHOD

Depending on the mechanical excitation applied to the tissues, there are mainly two approaches in US elastography, termed quasistatic elastography[19,24–26] and dynamic elastography.[18,27–29] This paper falls into the category of quasistatic elastography, which investigates tissue deformation under compression. In quasistatic elastography, information on tissue local mechanical properties is deduced from a simple principle: Subjected to a given stress, soft areas will deform more than stiffer ones. In practical terms, for a tissue under investigation, two US radiofrequency (RF) data sets are acquired, corresponding to two different stress levels called pre- and postcompression states. Pattern changes induced by the stress within the RF signals are then analyzed to compute a map of local strains.

The different steps leading to this local strain estimation are briefly explained hereafter to make the paper self-contained. The interested reader can refer to Refs. 26 and 30 for more details.

II.A. Image deformation model

To achieve a local estimation, images were divided into multiple small regions-of-interest (ROIs) and for each ROI, the effects of the tissue compression were analyzed. Most of the 2D techniques used in elastography model the compression-induced tissue motion as a local 2D translation and then compute strain as the gradient of the resulting displacement field. Contrary to these techniques, we considered that the effect of compression on each ROI can be modeled as an affine transformation. In addition to a 2D translation, a scaling of the ROI was also considered, which reflects more realistically the tissue deformation at this location.
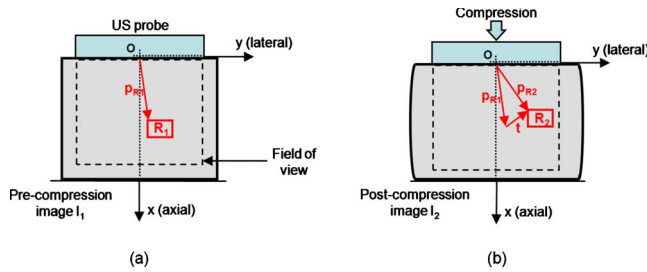
FIG. 1. Region of interest positioning in (a) the precompression image and (b) the postcompression image.

However, US data resolution is highly anisotropic. Owing to US device characteristics, lateral resolution is much coarser than the axial resolution, which makes an accurate estimation of a scaling factor difficult in the lateral direction. This has led us to consider only an axial scaling of the ROI, the lateral deformation being taken into account in the lateral translation of the ROI.

II.B. ROI displacement

Let us denote I_1 and I_2 the pre- and postcompression images, respectively. Let us consider R_1 a ROI of dimensions $L_{x1} \times L_{y1}$, located at p_{R1} in I_1. Finally, let us denote R_2 the ROI in I_2 corresponding to the same tissue region after deformation. Its axial and lateral dimensions L_{x2} and L_{y2} are such that $L_{x2} = \alpha \cdot L_{x1}$ (axial scaling) and $L_{y2} = L_{y1}$. The position of R_2 in I_2, namely, p_{R2}, is also different from p_{R1}, as shown in Fig. 1. We therefore initialize R_2 at its most probable position in I_2 as

$$p_{R2\text{ini}} = p_{R1} + t, \tag{1}$$

with $t(t_{ax}, t_{lat})$ a 2D translation. This translation vector represents the effects of tissue deformation on the position of R_2. In particular, its axial component t_{ax} results from the axial scaling of the regions located between the probe and the ROI currently considered. It can therefore be entirely determined from previous computations by beginning the estimation process for the regions at the interface with the probe (where $t_{ax} = 0$) and propagating this process to regions downward. Similarly, the lateral shift t_{lat} is directly given by the previous estimations, by beginning the estimation process for the regions at the center of the probe and propagating this process to the lateral sides.

II.C. Problem formulation

For the positions of R_1 and R_2 that have been determined, two local parameters must now be estimated: An axial scaling α and a residual lateral shift τ. This estimation is performed through the minimization of an objective function f, which is defined as the opposite of the normalized correlation coefficient between R_1 and R_2, R_2 varying with these parameters.

Since RF US data are oscillating signals by nature, the function f may exhibit several local minima. To narrow the optimization process around the area corresponding to the

global minimum, the range of values allowed for the parameters is reduced. This reduction in the parameter domain is reasonable since in elastography, deformations induced by the external load are of small magnitude (a few %). R_2 is therefore sought in a small region immediately surrounding its initial position. As a result, the optimization is subjected to a set of linear inequality constraints on the parameters and the problem to be solved can be formulated as

$$\begin{bmatrix} \hat{\alpha} & \hat{\tau} \end{bmatrix} = \arg\min_{\alpha, \tau} f(\alpha, \tau) \quad \text{with} \quad \begin{cases} \alpha_{min} \le \alpha \le \alpha_{max} \\ \tau_{min} \le \tau \le \tau_{max} \end{cases}. \tag{2}$$

Typically, axial strain is restricted to the range $[0\%-6\%]$ and lateral shift is limited to three times the RF line interspacing (i.e., $\alpha_{min} = 0.94$, $\alpha_{max} = 1$, $\tau_{min} = -3$, and $\tau_{max} = 3$).

In practical terms, this optimization process is implemented, thanks to a sequential quadratic programming methodology,[31] together with an active set strategy. To ensure a reliable estimation and prevent the objective function from being trapped in a local minimum, correction procedures are also considered based on multiple initializations of the process[26,30]

II.D. Axial strain computation

In this paper, the mechanical parameter we are interested in is the medium's axial strain. This information is directly deduced from the estimated axial scaling factor $\hat{\alpha}$, according to the following relation:

$$\varepsilon = \hat{\alpha} - 1. \tag{3}$$

It should be stressed that with Eq. (3), strain is negative for a compression and positive for a dilatation. Because in this study, all experiments were performed by applying a compression to the observed media, computed strain values were negative. For simplification purposes, we chose to display the opposite of the strain, leading to elastograms with positive values, keeping in mind that they represent the percentage of medium compression.

III. NUMERICAL SIMULATIONS

Deep pressure ulcers develop at the deepest level and proceeds outward until they reach the skin.[11,16,17] At an early stage of the pathology, deep tissues are therefore damaged while the epidermis is still intact. Besides, areas particularly exposed to pressure ulcers are those over bony prominences, such as the sacrum, hips, and heels, which represent 80% of bedsores.[32] From this background, a numerical phantom of pressure ulcer was designed with regard to these observations, and the potential of US elastography for the early detection of this condition was investigated.

The phantom of $30 \times 20 \times 4$ mm^3 modeled a deep ulcer at the very beginning of the pathological process (Fig. 2). It was made of three different regions:

- Healthy soft tissues in contact with the US probe,
- A bony prominence at the bottom, which is a privileged configuration for pressure ulcer formation,
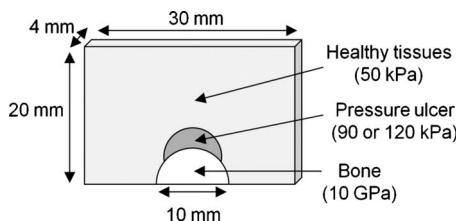
FIG. 2. Sketch of the numerical phantom mimicking a pressure ulcer at an early stage.
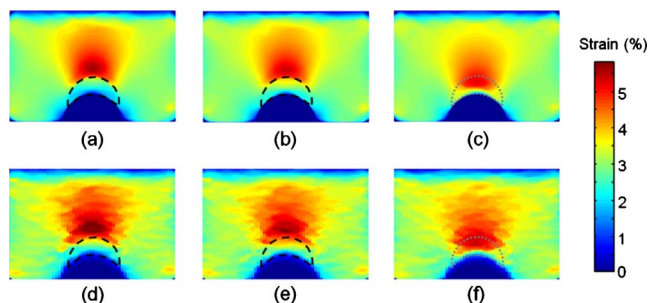

FIG. 3. Numerical phantom results. On the first row are the theoretical axial strain fields (given by the FEM) and on the second row are the estimated axial strain fields (in %). (a) and (d) are the fields for the configuration including a 120 kPa pressure ulcer. (b) and (e) are the fields for the configuration with a 90 kPa pressure ulcer. (c) and (f) are the fields for the configuration without pressure ulcer.

– And an intermediate layer mimicking the *in-development* ulcer, located above the bone, and whose limited size made it visually undetectable from the phantom upper surface.

The phantom mechanical properties were defined as follows: The Young's modulus of the bone was set to 10 GPa and that of healthy tissues was set to 50 kPa. These are orders of magnitude reported in literature.[33–35] The modeling of the pressure ulcer was based on the following observation. During their experiments, Gefen *et al.*[14] measured a 1.8–3.3-fold stiffening of tissues damaged by a pressure ulcer compared to normal ones. Accordingly, two different values were chosen for the Young's modulus of the pressure ulcer: Either 90 kPa, corresponding to the lowest ratio (1.8×50 kPa), or 120 kPa, corresponding to a middle range value. In addition, a third configuration was considered for control. It represented a "healthy" state, with no pressure ulcer (Young's modulus of 50 kPa).

To obtain the postcompression configuration, a 1.5 kPa stress was applied on the upper surface of phantoms downward. The corresponding tissue deformations were computed through the use of a finite element modeling (FEM) package (COMSOL MULTIPHYSICS, Comsol Inc., USA).

From an acoustical point of view, tissues were modeled as a large number of punctual scatterers randomly distributed in the region-of-interest. In the absence of information related to pressure ulcer echogenicity and since our technique is based only on tissue's stiffness differences, healthy and pathological tissues were considered as having identical acoustical properties. Consequently, a standard B-mode image did not allow seeing any difference between these two regions. On the other hand, the bone was designed to be hyperechoic compared to soft tissues.

US RF data were the result of the convolution between scatterers and a point spread function simulating the acoustical response of the scanner.[36] Simulations were performed for both the pre- and the postcompression states, displacements of scatterers between the two states being given by the FEM.

The strain estimator described in Sec. II was applied to these simulated data. The corresponding results, together with theoretical fields, are given in Fig. 3. We can first observe that the estimated elastograms are close to the theoretical fields provided by the FEM. They both exhibit similar patterns of strains, which is satisfying regarding the strain estimation method. The bone has a deformation close to zero, which is consistent with its stiffness, and it is clearly identified in the three elastograms. Its position also matches the hyperechoic region of the B-mode image. Although the pressure ulcer cannot be detected in the B-mode scan, the presence of a hard pathological area is revealed in the elastograms [Figs. 3(d) and 3(e)]: Strain for the pathological area is indeed half that of its upper neighborhood (about 2.5% vs 5%). Transitions from the healthy tissues to the ulcer and from the ulcer to the bone are very sharp. This underlines the hard region, with limits corresponding to the dotted line (area available from the FEM and added manually on the different maps). In contrast, the maps corresponding to the healthy model [Figs. 3(c) and 3(f)] show a relatively different configuration, with a smaller maximum and the region of highest strain overlapping the area of the ulcer.

IV. PRESSURE ULCER MIMICKING PHANTOM

In this section, additional tests are reported on a physical phantom designed to mimic an early stage pressure ulcer. A sketch of the phantom is shown in Fig. 4(a). It consisted of a $30 \times 60 \times 110$ mm³ parallelepiped, within which three regions can be identified: A bone, a region representing the in-development pressure ulcer, and the surrounding healthy tissues. The bone, of 10 mm in diameter, was a sample from the forward limb of a dog. Other regions were made of polyvinyl alcohol (PVA) cryogel. PVA cryogel is a polymer that was introduced in the 1990s to build phantoms mimicking soft tissues.[37] Mixed with Sigmacell particles (Sigmacell Cellulose, type 20, Sigma-Aldrich, USA), its acoustical properties are close to those of soft biological tissues, and this material is suitable for US imaging. Moreover, the material stiffness increases with the number of freeze-thaw cycles applied. By varying this number of cycles, a wide range of elasticity values can be obtained, especially those commonly met for soft biological tissues.[38,39] Since a pressure ulcer is stiffer than healthy tissues, the PVA cryogel for this region went through two freeze-thaw cycles, while the PVA cryogel for the healthy region underwent a single cycle. Such a pressure ulcer corresponds to a deep tissue injury.

RF US data were acquired with an *Ultrasonix Sonix RP* device (Ultrasonix Medical Corporation, Richmond, BC, Canada), equipped with a 7 MHz linear probe (reference
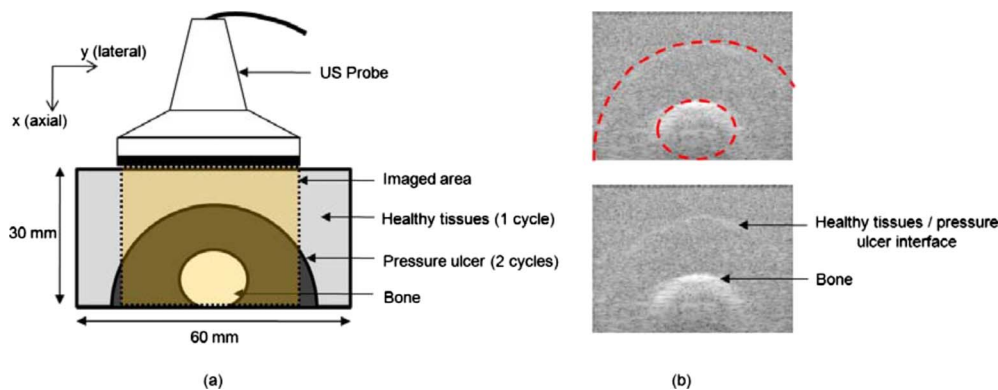
FIG. 4. (a) PVA phantom constitution. (b) B-mode image of the phantom.

L14-5/38). The postcompression data were acquired after uniform compression of the top surface of the phantom (applied with a plate, while the bottom surface remained fixed). These data were then processed with our strain estimator.

As it can be seen from the B-mode image of this region [Fig. 4(b)], the bone could be clearly identified from its specular reflection. However, the echography did not provide any information about the mechanical properties of the phantom. On the contrary, the estimated axial strain map (Fig. 5) was helpful for the detection of the three regions of the phantom. Even if strain values remained within a small range, it can be seen that pathological tissues exhibit a different pattern compared to the surrounding healthy soft tissues. Finally, deformation of the bone is almost negligible, as expected.

Mean strain were calculated for the different tissue types. They were equal to $1.01 \pm 0.24\%$, $0.45 \pm 0.16\%$, and $0.06 \pm 0.06\%$ for the healthy, pathological, and bone regions, respectively.

V. PRELIMINARY *IN VIVO* STUDY

To further evaluate the contribution of elastography for pressure ulcer detection, *in vivo* acquisitions on an experimental rat model were performed. The intent of this study was to investigate *in vivo* the ability of elastography to detect strain, when the tissues under examination were subjected to a long-term unrelieved pressure.

The main reason for tissue breakdown is ischemia,[11–13] in connection with the interface pressure at the skin level. Traditionally, the value of 32 mm Hg (4.3 kPa) is quoted for the pressure threshold that triggers capillary closure:[40] If maintained, interface pressures higher than this value are sup-

posed to lead to tissue damage. However, a more recent study demonstrates that this value is not relevant since capillary closure mainly depends on the local pressure.[41] To induce tissue breakdown, we therefore chose to adapt the protocol described by Gefen *et al.*,[14] where a maintained compression was applied on the thigh of rats to generate pressure ulcers. In the latter paper, it is shown that a pressure of 35 kPa maintained during 60 min leads to a twofold stiffening of tissues with cell death.

The protocol for animal experimentation was approved by the Animal Care Committee of the Centre Hospitalier de l'Université de Montréal, in accordance with the guidelines of the Canadian Council of Animal Care. The animal was an 18-week-old male rat from the Brown Norway breed and weighed 265 g. It was first anesthetized by inhalation of 2.5% isofluorane, the hair of the hind limb was carefully shaved, and the animal was then immobilized. Its body temperature was monitored with a rectal probe (Thermalert TH-5, Physitemp Instruments, Clifton, USA) and maintained at 37 ± 1 °C with a heating surface. A first set of RF US data
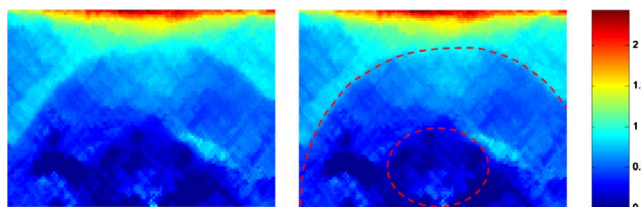

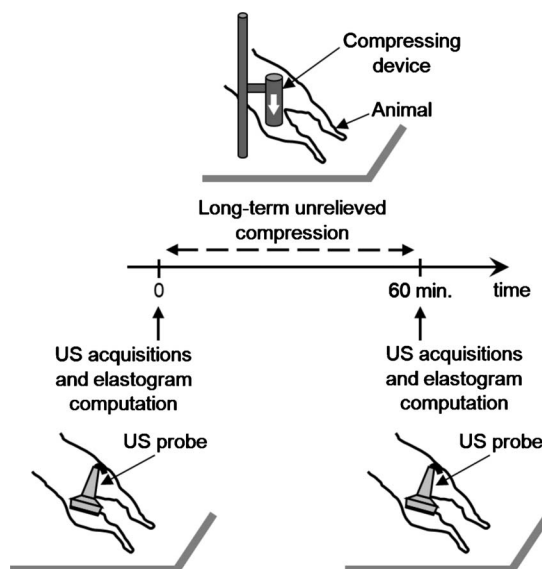FIG. 5. Estimated strain map (in %) for the PVA cryogel phantom.

FIG. 6. Scheme of the *in vivo* protocol used to induce a pressure ulcer early detection on a rat and to acquire US data for elastography imaging.
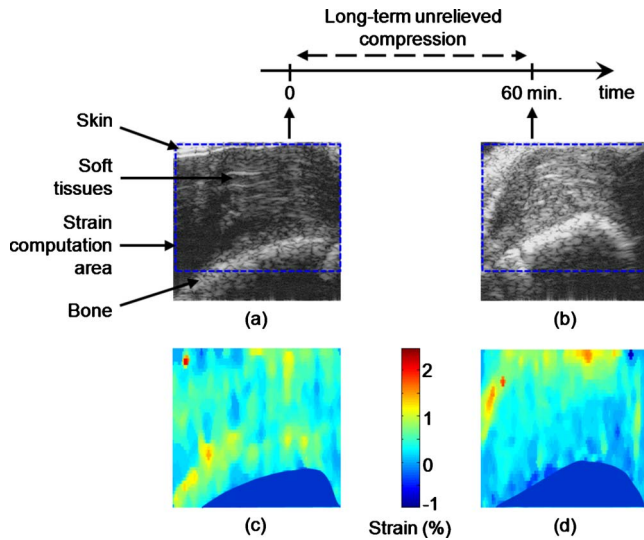
FIG. 7. B-mode images and elastograms for the *in vivo* experiment. (a) Initial B-mode image (showing the different tissues). (b) B-mode image after 60 min compression. (c) Initial elastogram. (d) Elastogram after 60 min compression.

TABLE I. Mean strain and standard deviation, according to time and location of the ROI, for the *in vivo* experiment.

Mean strain (%)		Time	
		0 min	60 min
ROI location	Close to the skin	0.48 ± 0.22	0.50 ± 0.27
	Close to the bone	0.47 ± 0.19	0.13 ± 0.13

different tissues can be identified: The skin, the bone (both hyperechoic), and soft tissues, which is the region that was specifically analyzed. The corresponding B-mode image after the application of the 60 min compression is shown in Fig. 7(b). Due to the 60 min compression, the B-mode images exhibit different patterns. However, these images alone are not relevant to reveal or not the presence of a pathological area. Computed elastograms are displayed in Figs. 7(c) and 7(d), respectively. The initial elastogram appears homogeneous. Only the area immediately above the bone exhibits a slightly higher strain. As a comparison, the same area on the second elastogram (i.e., after 60 min compression) behaved differently, with a deformation smaller than the surrounding tissues. A sharp evolution of the strain along depth is also visible for the whole image: Shallow tissues seem to exhibit higher strains compared to the tissues near the bone. This evolution tends to show that the tissue area over the bone became stiffer, which could be the indication of an emerging pressure ulcer.

To support this visual impression, mean deformations were calculated in two ROIs, as shown in Fig. 8. For a given image, both ROIs have the same size. They are also located at the same lateral position, but at different depths, either near the skin or near the bone. Mean strain was estimated over the pixels located within the perimeter defined by the ROI. The corresponding results are given in Table I. Before the compression was applied ($t=0$), the strain was almost the same for both regions (0.48% for the top ROI and 0.47% for the bottom ROI). On the other hand, mean strains were significantly different after the compression of 60 min: While the mean strain for the top ROI was 0.50%, that for the bottom ROI dropped to 0.13%. The large decrease in strain near the bone might be due to tissue stiffening in this region. This observation allows to assume that the area near the bone was pathological, corresponding to the presence of a pressure ulcer or, at least, corresponding to tissues that underwent a degradation such that they were significantly stiffer than healthy tissues.

was acquired, in a view to compute elastograms. A 35 kPa pressure was then applied on the thigh of the animal during 60 min to generate a pressure ulcer. A second set of RF US data was acquired after the 60 min compression. Once the experiments were completed, the animal was euthanized by inhalation of CO_2. Figure 6 summarizes the protocol.

RF US data were acquired with a *VisualSonics Vevo 660* device (VisualSonics Inc., Toronto, Canada), equipped with a 35 MHz probe dedicated to small animal studies. US data were acquired with the same settings of the scanner and were processed to compute elastograms before the application of the compression and after the 60 min compression. The compression tool was a wooden stick, whose end was a 2-cm-in-diameter disk in contact with the skin of the animal. Both the US probe and the compression device were mounted on a robotic arm (described in detail in Ref. 42). The latter was a 6 degrees of freedom industrial robot (F3 Articulated Robot, CRS Robotics Corporation, Burlington, Canada), equipped with a force sensor on its end (ATI, Industrial Automation, Apex, USA), and controlled through a software interface (Integral Technologies Inc., Laval, Canada). This enabled the control of the pressure applied with the compressing device and ensured an accurate positioning of the US probe.

Results of this experiment are presented in Fig. 7. Figure 7(a) provides a B-mode image of the investigated area where
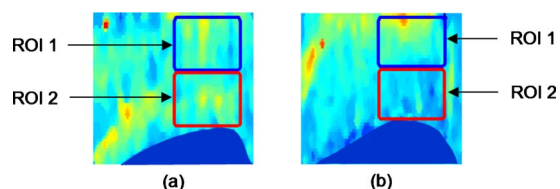
VI. DISCUSSION AND CONCLUSION

In this paper, we proposed a new approach based on ultrasound imaging to address the challenging problem of pressure ulcer early detection. Even though US elastography usually finds its main application in cancer tumor detection, we think it has great potential for pressure ulcer early detection. Since this pathology is associated with a stiffening of damaged tissues, highlighting abnormally hard areas could indeed be fundamental. Moreover, deep pressure ulcers are

FIG. 8. Location of the ROIs for mean strain computation (a) on the initial elastogram and (b) on the final elastogram.

characterized by a deep-to-superficial pattern: The ulcer develops in deep muscle tissues and progresses toward the skin. US elastography is therefore an interesting tool for early detection, when the deep ulcer is still imperceptible by visual inspection.

To investigate the usefulness of US elastography, different types of data were processed. Numerical simulations demonstrated that a pressure ulcer can theoretically be detected at a very early stage with US elastography. Even when the ulcer region was characterized by a low stiffening (ratio of 1.8 relative to normal tissues), the estimated elastogram clearly underlined the pathological area.

This observation was confirmed by the results obtained on a physical phantom mimicking a pressure ulcer at an early stage. Computed elastograms showed strain differences between areas mimicking healthy and pathological tissues.

Compared to the results on numerical data, these elastograms showed a different strain pattern, which could be attributed to the different designs of the simulated and experimental phantoms. Indeed, for building procedure reasons, the area mimicking the pressure ulcer in the physical phantom is much wider than those in simulations and completely covers the bone. However, both numerical and experimental results demonstrate that US elastography can detect an abnormally stiff area corresponding to a deep pressure ulcer in development, even though no particular symptom is visible on the skin.

Finally, *in vivo* experiments were conducted on a rat model. A maintained pressure was applied on the animal thigh during 60 min, with a view to generate a pressure ulcer. It has been shown in a previous study,[14] based on histologies, that the protocol used in our experiment (in particular, the same compressing device and level of pressure were considered) leads to irreversible muscle cell death after only 15 min of exposition. The same paper concludes that changes in mechanical properties follow morphological damages and cellular death. RF US data, acquired before and after application of this pressure, were processed with our strain estimator. Elastograms revealed a difference in the way tissues behaved before and after the pressure was applied, which strongly suggest the presence of a pathological area.

These first results naturally require confirmation by performing many other *in vivo* experiments. In particular, acquisitions on human patients can be envisaged using lower frequency probe to image a larger area of tissue.

Nevertheless, these first experiments demonstrate that US elastography is a promising technique for pressure ulcer detection, especially at an early stage of the pathology, when the disease is still visually undetectable. In the absence of any other technique, this is also a first step toward the development of an objective and reliable tool.

[a]Electronic mail: jean-francois.deprez@eng.ox.ac.uk

[1]National Pressure Ulcer Advisory Panel, "Pressure ulcers in America: Prevalence, incidence, and implications for the future. An executive summary of the National Pressure Ulcer Advisory Panel monograph," Adv. Skin Wound Care **14**(4), 208–215 (2001).

[2]K. O'Dea, "Prevalence of pressure damage in hospital patients in the UK," J. Wound Care **2**, 221–225 (1993).

[3]S. E. Sedory Holzer, A. Camerota, L. Martens, T. Cuerdon, J. Crystal-Peters, and M. Zagari, "Costs and duration of care for lower extremity ulcers in patients with diabetes," Clin. Ther. **20**(1), 169–181 (1998).

[4]H. Miller and J. Delozier, "Cost implications of the pressure ulcer treatment guideline," Columbia, MD, Center for Health Policy Studies, 1994:17, Contract 2282-91-0070 (1994).

[5]I. Cho and M. Noh, "Braden scale: Evaluation of clinical usefulness in an intensive care unit," J. Adv. Nurs. **66**(2), 293–302 (2010).

[6]R. J. Goldman and R. Salcido, "More than one way to measure a wound: An overview of tools and techniques," Adv. Skin Wound Care **15**, 236–243 (2002).

[7]A. A. Weber, C. Gehin, G. Moddy, J. Jossinet, and E. T. McAdams, "Characterization of a multi-frequency wound impedance mapping instrument," Proceedings of the 30th IEEE EMBS Conference, Vancouver, Canada, 20–24 August, 2008.

[8]S. Treuillet, B. Albouy, and Y. Lucas, "Three-dimensional assessment of skin wounds using standard digital camera," IEEE Trans. Med. Imaging **28**(5), 752–762 (2009).

[9]E. S. Andersen and T. Karlsmark, "Evaluation of four non-invasive methods for examination and characterization of pressure ulcers," Skin Res. Technol. **14**, 270–276 (2008).

[10]R. Meffre, C. Gehin, P. M. Schmitt, F. De Oliveira, and A. Dittmar, "New methodology for preventing pressure ulcers using actimetry and autonomous nervous system recording," Proceedings of the 28th IEEE EMBS Conference, New York, NY, 30 August–3 September 2006 (unpublished).

[11]R. K. Daniel, D. L. Priest, and D. C. Weatley, "Etiological factors in pressure sores: An experimental model," Arch. Phys. Med. Rehabil. **62**, 492–498 (1981).

[12]S. M. Dinsdale, "Decubitus ulcers: Role of pressure and friction in causation," Arch. Phys. Med. Rehabil. **55**, 147–152 (1974).

[13]M. Kosiak, "Etiology of decubitus ulcers," Arch. Phys. Med. Rehabil. **42**, 19–29 (1961).

[14]A. Gefen, N. Gefen, E. Linder-Ganz, and S. S. Margulies, "In vivo muscle stiffening under bone compression promotes deep pressure sores," J. Biomech. Eng. **127**, 512–524 (2005).

[15]E. Linder-Ganz and A. Gefen, "Stress analyses coupled with damage laws to determine biomechanical risk factors for deep tissue injury during sitting," J. Biomech. Eng. **131**(1), 011003 (2009).

[16]C. V. Bouten, C. W. Oomens, F. P. Baaijens, and D. L. Bader, "The etiology of pressure ulcer: Skin deep or muscle bound?," Arch. Phys. Med. Rehabil. **84**, 616–619 (2003).

[17]C. W. J. Oomens, S. Loerakker, and D. L. Bader, "The importance of internal strain as opposed to interface pressure in the prevention of pressure related deep tissue injury," J. Tissue Viability **19**(2), 35–42 (2010).

[18]T. A. Krouskop, D. R. Dougherty, and S. F. Levinson, "A pulsed Doppler ultrasonic system for making noninvasive measurements of the mechanical properties of soft tissue," J. Rehabil. Res. Dev. **24**, 1–8 (1987).

[19]J. Ophir, I. Céspedes, H. Ponnekanti, Y. Yazdi, and X. Li, "Elastography: A quantitative method for imaging the elasticity of biological tissues," Ultrason. Imaging **13**, 111–134 (1991).

[20]M. Tanter, J. Bercoff, A. Athanasiou, T. Deffieux, J. L. Gennisson, G. Montaldo, M. Muller, A. Tardivon, and M. Fink, "Quantitative assessment of breast lesion viscoelasticity: Initial clinical results using supersonic shear imaging," Ultrasound Med. Biol. **34**, 1373–1386 (2008).

[21]K. Konig, U. Scheipers, A. Pesavento, A. Lorenz, H. Ermert, and T. Senge, "Initial experiences with real-time elastography guided biopsies of the prostate," J. Urol. (Paris) **174**, 115–117 (2005).

[22]L. Sandrin, B. Fourquet, J. M. Hasquenoph, S. Yon, C. Fournier, F. Mal, C. Christidis, M. Ziol, B. Poulet, F. Kazemi, M. Beaugrand, and R. Palau, "Transient elastography: A new noninvasive for assessment of hepatic fibrosis," Ultrasound Med. Biol. **29**(12), 1705–1713 (2003).

[23]R. L. Maurice, J. Ohayon, Y. Frétigny, M. Bertrand, G. Soulez, and G. Cloutier, "Noninvasive vascular elastography: Theoretical framework," IEEE Trans. Med. Imaging **23**(2), 164–180 (2004).

[24]S. K. Alam, J. Ophir, and E. Konofagou, "An adaptive strain estimator for elastography," IEEE Trans. Ultrason. Ferroelectr. Freq. Control **45**, 461–472 (1998).

[25]E. Brusseau, C. Perrey, P. Delachartre, M. Vogt, D. Vray, and H. Ermert, "Axial strain imaging using a local estimation of the scaling factor from RF ultrasound signals," Ultrason. Imaging **22**(2), 95–107 (2000).

[26]E. Brusseau, J. Kybic, J. F. Deprez, and O. Basset, "2D locally regularized tissue strain estimation from radio-frequency ultrasound images: theoretical developments and results on experimental data," IEEE Trans.

Med. Imaging **27**(2), 145–160 (2008).

[27]A. P. Sarvazyan, O. V. Rudenko, S. D. Swanson, J. B. Fowlkes, and S. Y. Emelianov, "Shear wave elasticity imaging—A new ultrasonic technology of medical diagnostic," Ultrasound Med. Biol. **24**, 1419–1435 (1998).

[28]K. Nightingale, M. S. Soo, R. Nightingale, and G. Trahey, "Acoustic radiation force impulse imaging: In vivo demonstration of clinical feasibility," Ultrasound Med. Biol. **28**, 227–235 (2002).

[29]J. Bercoff, M. Tanter, and M. Fink, "Supersonic shear imaging: A new technique for soft tissue elasticity mapping," IEEE Trans. Ultrason. Ferroelectr. Freq. Control **51**(4), 396–409 (2004).

[30]J. F. Deprez, E. Brusseau, C. Schmitt, G. Cloutier, and O. Basset, "3D estimation of soft biological tissue deformation from radio-frequency ultrasound volume acquisitions," Med. Image Anal. **13**, 116–127 (2009).

[31]P. T. Boggs and J. W. Tolle, "Sequential quadratic programming," Acta Numerica **4**, 1–51 (1995).

[32]B. Barrois, L. Heitler, and P. Ribinik, *L'escarre: Les basiques* (Edition Asymptote, Paris, 1999).

[33]J. Y. Rho, R. B. Ashman, and C. H. Turner, "Young's modulus of trabecular and cortical bone material: Ultrasonic and microtensile measurements," J. Biomech. **26**(2), 111–119 (1993).

[34]B. K. Hoffmeister, S. R. Smith, S. M. Handley, and J. Y. Rho, "Anisotropy of Young's modulus of human tibial cortical bone," Med. Biol. Eng. Comput. **38**(3), 333–338 (2000).

[35]T. A. Krouskop, T. M. Wheeler, F. Kallel, B. S. Garra, and T. Hall, "Elastic moduli of breast and prostate tissues under compression," Ultrason. Imaging **20**, 260–274 (1998).

[36]J. Meunier and M. Bertrand, "Ultrasonic texture motion analysis: Theory and simulation," IEEE Trans. Med. Imaging **14**(2), 293–300 (1995).

[37]K. C. Chu and B. K. Rutt, "Polyvinyl alcohol cryogel: An ideal phantom material for MR studies of arterial flow and elasticty," Magn. Reson. Med. **37**(2), 314–319 (1997).

[38]J. Fromageau, E. Brusseau, D. Vray, G. Gimenez, and P. Delachartre, "Characterization of PVA cryogel for intravascular ultrasound elasticity imaging," IEEE Trans. Ultrason. Ferroelectr. Freq. Control **50**(10), 1318–1324 (2003).

[39]J. Fromageau, J. L. Genisson, C. Schmitt, R. L. Maurice, R. Mongrain, and G. Cloutier, "Estimation of polyvinyl alcohol cryogel mechanical properties with four ultrasound elastography methods and comparison with gold standard testings," IEEE Trans. Ultrason. Ferroelectr. Freq. Control **54**(3), 498–509 (2007).

[40]E. M. Landis, "Micro-injection studies of capillary blood pressure in human skin," Heart **15**, 209–228 (1930).

[41]D. L. Bader, "The recovery characteristics of soft tissues following repeated loading," J. Rehabil. Res. Dev. **27**, 141–150 (1990).

[42]M. A. Janvier, L. G. Durand, M. H. Roy Cardinal, I. Renaud, B. Chayer, P. Bigras, J. de Guise, G. Soulez, and G. Cloutier, "Performance evaluation of a medical robotic 3D-ultrasound imaging system," Med. Image Anal. **12**, 275–290 (2008).